Frontiers of Information Technology & Electronic Engineering
www.jzus.zju.edu.cn; engineering.cae.cn; www.springerlink.com
ISSN 2095-9184 (print); ISSN 2095-9230 (online)
E-mail: jzus@zju.edu.cn

Sb_2Te_3 topological insulator for 52 nm wideband tunable Yb-doped passively Q-switched fiber laser*

Tao WANG[§1], Qiang YU[§1,2], Kun GUO[1], Xinyao SHI[2], Xuefen KAN[3], Yijun XU[4,5], Jian WU[†‡1,4], Kai ZHANG[†‡2], Pu ZHOU[1]

[1]*College of Advanced Interdisciplinary Studies, National University of Defense Technology, Changsha 410073, China*
[2]*i-Lab, Suzhou Institute of Nano-Tech and Nano-Bionics, Chinese Academy of Sciences, Suzhou 215123, China*
[3]*Jiangsu Key Laboratory of Power Transmission and Distribution Equipment Technology, Hohai University, Changzhou 213022, China*
[4]*Key Laboratory of Nano-Devices and Applications, Suzhou Institute of Nano-Tech and Nano-Bionics, Chinese Academy of Sciences, Suzhou 215123, China*
[5]*Vacuum Interconnected Nanotech Workstation, Suzhou Institute of Nano-Tech and Nano-Bionics, Chinese Academy of Sciences, Suzhou 215123, China*
[†]E-mail: wujian15203@163.com; kzhang2015@sinano.ac.cn

Received Oct. 26, 2020; Revision accepted Dec. 23, 2020; Crosschecked Jan. 22, 2021

Abstract: Topological insulator Sb_2Te_3 has the advantage of broadband saturable absorption from the visible to the infrared bands. Herein, the two-dimensional material Sb_2Te_3 saturable absorber (SA) of the topological insulator family was first applied experimentally in a wideband tunable passively Q-switched Yb-doped fiber laser. High-quality Sb_2Te_3 crystals were synthesized by the flux zone method. The Sb_2Te_3 SA with fewer layers was further prepared via a modified mechanical exfoliation procedure. Meanwhile, stable wavelength-tunable passive Q-switching pulse operation was obtained in a Yb-doped fiber ring cavity based on the Sb_2Te_3 SA, where the central wavelength can be continuously tuned from 1040.89 to 1092.85 nm. Results suggest that Sb_2Te_3 has wideband saturable absorption properties, and that the tunable pulse laser can provide a convenient and simple source for practical applications.

Key words: Topological insulator; Sb_2Te_3; Fiber laser; Passive Q-switching laser; Wavelength-tunable laser
https://doi.org/10.1631/FITEE.2000577 **CLC number:** TB3

1 Introduction

Owing to their excellent nonlinear optical characteristics, tunable energy bandgap, and easy processing, various two-dimensional (2D) and quasi-2D materials have become popular choices as modulators in optical devices and pulse fiber laser generation in the past few years, such as graphene (Bao et al., 2009; Bonaccorso et al., 2010), black phosphorus (BP) (Hisyam et al., 2017; Wang T et al., 2019c), transition metal dichalcogenides (TMDs) (Xia et al., 2015; Liu WJ et al., 2018; Yang et al., 2019), and other 2D materials (Guo J et al., 2020; Guo PL, 2020; Li et al., 2020; Zhang Q et al., 2020; Zhang Y, 2020b, 2020c). Recently, topological insulators (TIs) have also been widely applied in pulsed fiber laser systems (Luo et al., 2013; Lin et al., 2015; Jhon et al., 2018; Rong et al., 2018) because of their unique optical and electrical characteristics (Hsieh et al., 2008). These possess a graphene-like energy band structure with a

‡ Corresponding authors
§ These authors contributed equally to this work
* Project supported by the National Natural Science Foundation of China (Nos. 61875223 and 61801472), the Hunan Province Key Area Research and Development Plan (No. 2019GK2181), the Hunan Provincial Innovation Project (No. 2019RS3017), and the Postgraduate Research & Practice Innovation Program of Jiangsu Province, China (Nos. B200203143 and KYCX20_0433)
ORCID: Jian WU, https://orcid.org/0000-0003-3747-7358; Kai ZHANG, https://orcid.org/0000-0001-9378-0947

small bulk state bandgap (0.2–0.3 eV) (Hsieh et al., 2008; Zhang HJ et al., 2009), which enables the potential of broadband absorption extending from visible light to infrared band. Moreover, it has been experimentally evidenced that TIs have saturable absorption not only in the optical band, but also in the microwave/terahertz band (Chen SQ et al., 2014), compared with other novel materials such as antimonene (Wang YZ et al., 2019), MXene (Huang WC et al., 2020; Wu Q et al., 2020), SnS (Wu LM et al., 2018; Xie et al., 2019), and Se (Xing et al., 2017). Researchers are constantly seeking potential candidates for next-generation optoelectronic devices (Qiu et al., 2013, 2015, 2016; Huang HY et al., 2016; Xiong, 2019). TIs have also been employed in high-performance photodetectors in recent years due to their photodetection characteristics (Zhang Y et al., 2019, 2020a). As a typical TI that possesses saturable absorption and giant third-order nonlinearity characteristics, Sb_2Te_3 has also been widely investigated for pulsed laser (Sotor et al., 2014a; Kowalczyk et al., 2016; Liu WJ et al., 2016). It has a refractive coefficient of up to 10^{-9} m^2/W (Liu J et al., 2010), which is at least four orders of magnitude larger than that of graphene (10^{-13} m^2/W) (Zhang H et al., 2012). The first mechanically exfoliated Sb_2Te_3 based Er-doped mode-locked fiber laser was achieved by Sotor et al. (2014b). Liu WJ et al. (2015) demonstrated a dark soliton Er-doped fiber laser by incorporation of the Sb_2Te_3 saturable absorber (SA). Furthermore, Yan et al. (2016) fabricated a Sb_2Te_3 saturable absorption mirror and achieved Q-switched pulse output. Later, the Sb_2Te_3 SA was first applied at 2 μm regime in a pulsed fiber laser (Wang JT et al., 2018). Next, a Sb_2Te_3 based harmonic mode-locking ultrafast fiber laser was presented (Wang ZH et al., 2019). These results indicate that Sb_2Te_3 SA can be applied as a fiber device for various methods of pulsed laser generation with excellent optical performance.

Wavelength-tunable laser sources have attracted a lot of attention due to the pressing need in spectroscopy, optical communication, biomedical science, and other fields (Zhang H et al., 2010; Meng et al., 2015; Liang et al., 2016; Lü et al., 2019). Wavelength-tunable Q-switched fiber lasers based on various 2D SAs have been widely investigated, but most of them operate at the 1.5 μm region (Popa et al., 2011; Cao et al., 2012; Chen Y et al., 2014; Huang YZ et al., 2014; Ahmad et al., 2015; Xia et al., 2015). As for the 1 μm waveband, Woodward et al. (2014) achieved a passive Q-switching laser with 40 nm of tunability based on MoS_2 in Yb-doped fiber (YDF). Ahmad et al. (2016) reported a Q-switched fiber laser with a tunable range of 1056.6 to 1083.3 nm by the incorporation of BP. Wu HS et al. (2017) achieved a trilaminar graphene based Q-switching YDF laser with an operating range of over 70 nm. Recently, Wang T et al. (2019d) also presented a wavelength-tunable high-order mode Q-switched laser in YDF based on BP. Wavelength-tunable Q-switched lasers have been achieved in the 1.5 μm region by applying TIs (Chen Y et al., 2014; Ahmad et al., 2015). Nevertheless, no reports on Yb-doped fibers have emerged. Compared with other results based on TIs, especially Sb_2Te_3, the present work has successfully realized wavelength-tunable Q-switched pulses in the 1 μm waveband for the first time.

The broadband saturable absorption properties make Sb_2Te_3 an excellent SA for tunable fiber lasers. Based on these properties, a stable wideband tunable passive Q-switching operation is demonstrated herein through incorporation of the Sb_2Te_3 SA. This Q-switched laser has tunability of more than 50 nm from 1040.89 to 1092.85 nm. Furthermore, the results presented in this paper extend the possible applications of Sb_2Te_3 to nonlinear optics and SA devices.

2 Sample preparation and experimental setup

2.1 Crystal growth and SA preparation

High-quality Sb_2Te_3 crystals were synthesized via the flux zone method. Considering that the raw material has a high melting point and is difficult to volatilize and transport, this method is more conducive to Sb_2Te_3 synthesis than chemical vapor transport or other methods (Huang WC et al., 2018a, 2018b, 2019). Typically, a stoichiometric amount of Te powder (99.999%, Alfa Aesar, USA, in 5% excess) and Sb powder (99.999%, Alfa Aesar, USA) weighing 1 g in total were mixed and sealed in an evacuated quartz glass tube with 200 mm length and 16 mm inner diameter under 10^{-3} Pa vacuum atmosphere. The tube was then vertically put in a muffle furnace and heated to 900 °C at a rate of 1 °C/min. After maintaining the temperature at 900 °C for 24 h, it was

decreased to 550 °C within 48 h and held at this value for another 72 h. Subsequently, the furnace was left at room temperature to cool down naturally. After several attempts, the growth temperature was proved as a more important factor than the cooling rate for crystallization. The resulting Sb_2Te_3 thin film SA was transferred onto the end face of a fiber ferrule by the modified Scotch tape mechanical exfoliation procedure. Thus, a Sb_2Te_3 based SA device was implemented.

2.2 Sample characterization

A field-emission scanning transmission electron microscope (Tecnai G2 F20 S-Twin, FEI, USA) was used to capture the transmission electron microscopy (TEM) images and acquire the electron diffraction (SAED) patterns of the selected area. The morphology of mechanically stripped Sb_2Te_3 nanosheets was characterized by scanning electron microscope (SEM, Quanta 250, FEI, USA). An X-ray diffractometer system (AXS D8 Advance, Bruker, USA) with Cu Kα irradiation (λ=0.154 06 nm) was adopted to record the X-ray diffraction (XRD) spectra. Raman spectroscopy was carried out using an instrument (LabRAM HR Evolution, HORIBA, France) with the excitation of 532 nm through a 100× objective.

As shown in Fig. 1, TEM was used to characterize the crystal structure of Sb_2Te_3 samples prepared by the ultrasonic dispersion method; it was shown thicker than mechanically stripped samples. A typical TEM image of the Sb_2Te_3 sample is depicted in Fig. 1a. Fig. 1b presents a high-resolution TEM image, illustrating that the planar distance of lattice fringes is 0.214 nm, which corresponds to the (110) direction shown in the SAED pattern of Fig. 1d. The high-angle annular dark-field scanning transmission electron microscopy (HAADF-STEM) and corresponding energy dispersive X-ray (EDX) mappings, demonstrated in Figs. 1c–1f, indicate that the Sb and Te atoms are evenly distributed in the whole material, showing good chemical uniformity.

The SEM image (Fig. 2a) reveals a layered morphology and smooth surface of the grown Sb_2Te_3 nanosheet. The corresponding elemental analysis and EDX mappings (Figs. 2b–2d) indicate that the Sb atoms and Te atoms are homogeneously distributed in the whole Sb_2Te_3 crystal with atomic ratios of 40.72% (Sb) and 59.28% (Te) in a ratio of approximately 2:3,

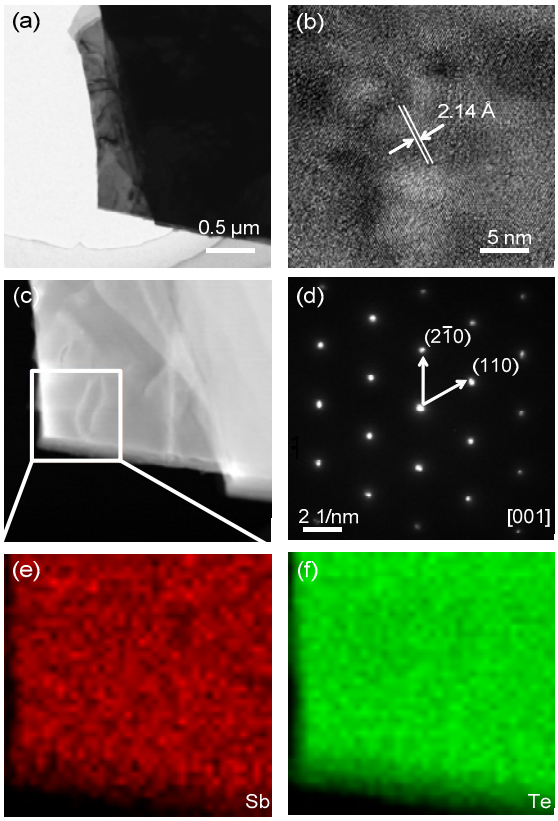

Fig. 1 Transmission electron microscopy (TEM) characterization of the Sb_2Te_3 sample: (a) TEM image of the Sb_2Te_3 sample on a copper grid; (b) high-resolution TEM image of the Sb_2Te_3 sample; (c) HAADF-STEM image; (d) corresponding SAED pattern showing its single crystal nature; (e) elemental mapping of Sb; (f) elemental mapping of Te

which confirms that the Sb_2Te_3 crystal is well synthesized. The XRD spectra show the main characteristic peaks of high crystalline Sb_2Te_3 (Fig. 2e). The peaks of (003), (006), (0012), (0015), and (0018) in Sb_2Te_3 are consistent with the standard card PDF#15-0874. The Raman spectrum of Sb_2Te_3 is presented in Fig. 2f, showing characteristic peaks at 65, 109, and 162 cm^{-1}, corresponding to A^1_g, E^2_g, and A^2_g vibration modes, respectively.

Moreover, the nonlinear saturation absorption properties of Sb_2Te_3 SA were characterized by a power-dependent transmission technique, as described previously (Wang T et al., 2019a, 2019b). The seed laser is a commercial pulsed laser (with a central wavelength of 1060 nm and a pulse width of 400 ps). The measurement data are shown in Fig. 3, meeting the properties described below (Garmire, 2000):

$$T(I)=1-\frac{\alpha_s}{1+I/I_{sat}}-\alpha_{ns},$$

where $T(I)$ represents the transmittance, α_s the modulation depth, α_{ns} the unsaturated loss, I the incident light intensity, and I_{sat} the saturated intensity. The fitting modulation depth and saturated intensity are 4.1% and 5.8 MW/cm^2, respectively, as shown by the fitting curve.

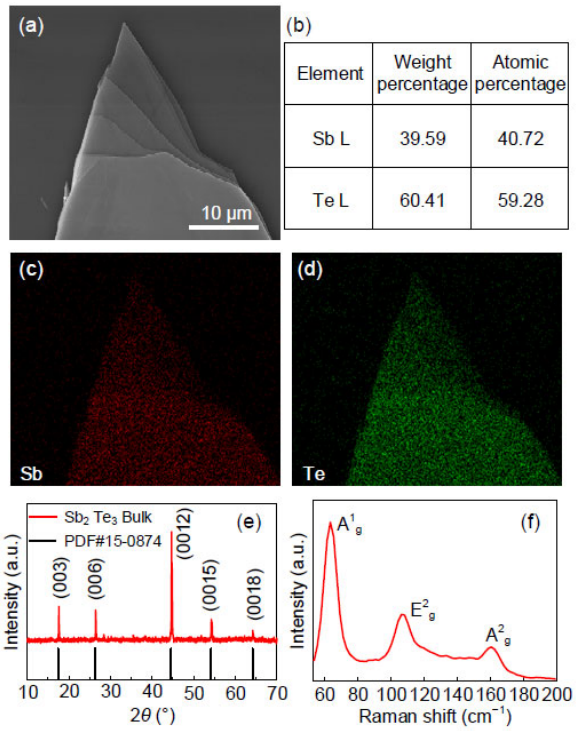

Fig. 2 Characterization of as-grown samples: (a) SEM image of a randomly selected Sb_2Te_3 nanosheet; (b) corresponding elemental analysis of this Sb_2Te_3 nanosheet; (c) EDX element mappings for Sb; (d) EDX element mappings for Te; (e) XRD pattern; (f) Raman spectrum of the Sb_2Te_3 nanosheet

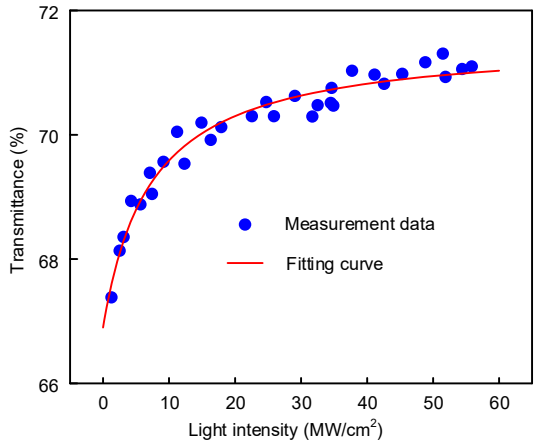

Fig. 3 Nonlinear transmittance of the Sb_2Te_3 saturable absorber at different light intensities

2.3 Experimental setup

The experimental schematic is presented in Fig. 4. The active fiber was a piece of YDF with 2 m length. The pump light was provided by a 976 nm laser diode (LD), and coupled into the cavity via wavelength division multiplexing (WDM) at 976/1064 nm. A polarization-insensitive isolator (PI-ISO) was connected into the cavity to enable unidirectional laser circulation. A tunable filter (TF) (filter bandwidth of about 1 nm) was used to function as a spectral filter. A polarization controller (PC) was integrated between the TF and the coupler to adjust the polarization. Ten percent of the coupler arm was adopted to extract the energy. The Sb_2Te_3 SA was connected between the WDM and the coupler to construct the ring cavity and induce pulsed laser operation. The total length of cavity was about 32.5 m. The output laser was characterized by a power meter, a digital oscilloscope (1 GHz bandwidth), and an optical spectrum analyzer (0.02 nm resolution).

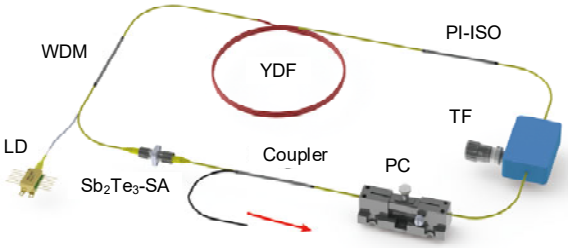

Fig. 4 Experimental setup for the Sb_2Te_3 SA based wavelength-tunable passive Q-switching YDF laser
SA: saturable absorber; YDF: Yb-doped fiber; LD: laser diode; WDM: wavelength division multiplexing; PI-ISO: polarization-insensitive isolator; TF: tunable filter; PC: polarization controller

3 Results and discussion

Based on the experimental schematic presented above, a broadband wavelength-tunable passive Q-switching YDF laser could be realized with the aid of the TF. The output laser wavelength could be tuned continuously from 1040.89 to 1092.85 nm by

adjusting the TF. Once the output wavelength was adjusted <1040.89 nm or >1092.85 nm, only continuous wave (CW) output could be achieved. The adjustable wavelength range of the Q-switched laser was limited by the overall loss of cavity rather than the TF, which had a tunable range of over 80 nm. The spectra at 12 typical different wavelengths within the tunable range are presented in Fig. 5a. No apparent difference could be observed in the linewidths at different wavelengths. Fig. 5b shows the pulsed lasing threshold at each selected wavelength. The threshold was as low as 240.6 mW at 1060.18 nm, and reached the maximum value of 336.1 mW at 1092.85 nm. At a fixed pump power of 379.6 mW, the maximum output power among different wavelengths was 9.6 mW at 1060.18 nm, and it declined at shorter and longer wavelengths (Fig. 5c). The difference in pulse thresholds and output power under the same pump power is caused by the combination of wavelength-dependent active fiber gain and optical device loss.

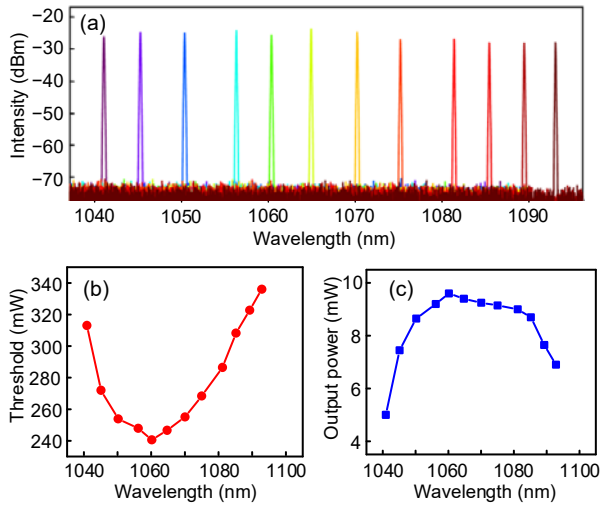

Fig. 5 Pulse characteristics at different wavelengths: (a) spectra; (b) pulse threshold; (c) output power

Next, we investigated the properties of passive Q-switching pulsed laser in detail (λ=1060.77 nm). The CW was observed first at a pump power of 159.6 mW. As it was further increased to 217.6 mW, the Q-switched pulse could be obtained, but the pulse was not stable at this state until the pump power reached 241.8 mW. The output power was proportional to the pump power, and peaked at 10.0 mW at the pump power of 386.8 mW (Fig. 6a). Meanwhile, the Q-switched pulse became unstable when the pump power further increased from 241.8 to above 386.8 mW. This increase led to a gradually increased repetition rate from 26.05 to 33.96 kHz and a decreased pulse width from 10.69 to 3.99 μs (Fig. 6b). The relationship between pump power and single pulse energy is depicted in Fig. 6c. The maximum value of single pulse energy at the maximum pump power was 294.5 nJ. The corresponding peak power at different values of pump power is presented in Fig. 6d. The increase in pump power led to a gradual increase in peak power, with the maximum value of 73.74 mW.

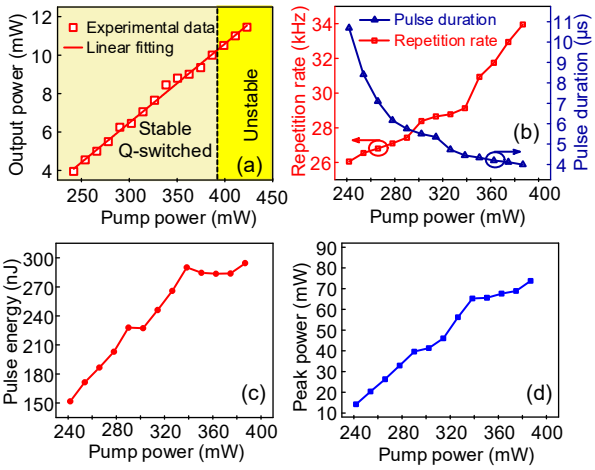

Fig. 6 Q-switched laser properties at 1060.8 nm output wavelength: (a) output power recorded by a power meter; (b) pulse width and repetition rate of pulse train at different values of pump power; (c) pulse energy; (d) peak power

The Q-switched laser properties were also recorded at a fixed pump power of 314.3 mW. Fig. 7a presents the output spectrum centered at 1060.77 nm, leading to a bandwidth of 0.11 nm. The pulse train for the output spectrum with a pulse interval of 34.9 μs is depicted in Fig. 7b. Fig. 7c plots the pulse profile, displaying a pulse width of about 5.35 μs as fitted by the Gaussian function. The radio frequency (RF) signal of the Q-switched laser was also measured. Fig. 7d shows the repetition rate measured as 28.65 kHz, with a signal-to-noise ratio (SNR) of 52.1 dB. The inset shows the RF trace spanning 300 kHz, indicating excellent temporal stability.

A relatively complete performance summary of wavelength-tunable Q-switching YDF based on different SAs is detailed in Table 1. Various optical

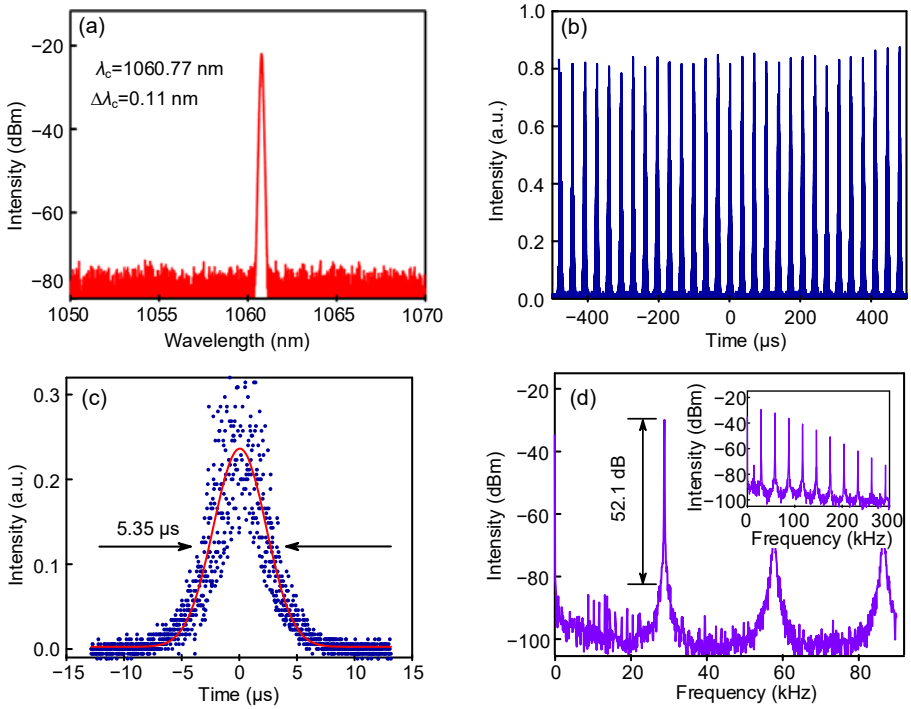

Fig. 7 Pulse properties at fixed pump power: (a) output spectrum centered at 1060.77 nm; (b) pulse train; (c) pulse duration; (d) RF spectra where the inset RF trace ranges from 0 to 300 kHz

Table 1 Comparison of wavelength-tunable passive Q-switching YDF based on different SAs

Saturable absorber	Reference	Wavelength (nm)	Maximum output power (mW)	Repetition rate (kHz)	Minimum pulse width (μs)	SNR (dB)
MoS_2	Woodward et al. (2014)	1030.00–1070.00	10.50	65.30–89.00	2.68	45.00
BP	Ahmad et al. (2016)	1056.60–1083.30	>0.30	6.00–44.80	4.00	52.00
Graphene	Wu HS et al. (2017)	1020.00–1090.40	>30.00	–	2.79	49.80
BP	Wang T et al. (2019d)	1054.40–1068.20	9.95	15.46–24.59	4.21	37.00
Sb_2Te_3	The present work	1040.89–1092.85	10.00	26.05–33.96	3.99	52.10

modulators, including MoS_2, BP, graphene, and Sb_2Te_3, have been employed to generate wavelength-tunable pulse. In this work, comparatively large SNR and mediate wavelength tunability range were obtained. In addition, the pulse laser was realized with the largest wavelength at 1092.9 nm. This result indicates that Sb_2Te_3 SA has the potential to output stable wideband pulses.

4 Conclusions

A broadband tunable passive Q-switching YDF laser based on Sb_2Te_3 was experimentally demonstrated for the first time. The Sb_2Te_3 SA was successfully fabricated with the flux zone method and a modified mechanical exfoliation procedure. The wideband saturable absorption properties of Sb_2Te_3 enabled a Q-switched pulse operation range of 1040.89 to 1092.85 nm. However, an even larger central wavelength tunability range can be expected if the cavity loss is further improved. The output power, repetition rate, pulse duration, pulse train, RF signal, pulse energy, and peak power of the Q-switching pulse were recorded in detail at the wavelength of 1060.77 nm. Our results suggest that Sb_2Te_3 has wideband saturable absorption properties. With a simple and convenient configuration, this broadband tunable passive Q-switching fiber laser can be highly attractive for applications in optical communication, biomedical diagnostics, environmental sensing, and other fields.

Contributors

Jian WU, Kai ZHANG, and Pu ZHOU conceived and designed the research. Tao WANG, Qiang YU, Kun GUO, Xinyao SHI, Yijun XU, and Xuefen KAN performed the experiments. Tao WANG and Qiang YU analyzed the data and drafted the manuscript. Jian WU, Kai ZHANG, and Pu ZHOU helped organize the manuscript. Tao WANG, Qiang YU, Xinyao SHI, Jian WU, Kai ZHANG, and Pu ZHOU revised and finalized the manuscript.

Compliance with ethics guidelines

Tao WANG, Qiang YU, Kun GUO, Xinyao SHI, Xuefen KAN, Yijun XU, Jian WU, Kai ZHANG, and Pu ZHOU declare that they have no conflict of interest.

References

Ahmad H, Soltanian MRK, Narimani L, et al., 2015. Tunable S-band Q-switched fiber laser using Bi_2Se_3 as the saturable absorber. *IEEE Photon J*, 7(3):1502508. https://doi.org/10.1109/JPHOT.2015.2433020

Ahmad H, Salim MAM, Thambiratnam K, et al., 2016. A black phosphorus-based tunable Q-switched ytterbium fiber laser. *Laser Phys Lett*, 13(9):095103. https://doi.org/10.1088/1612-2011/13/9/095103

Bao QL, Zhang H, Wang Y, et al., 2009. Atomic-layer graphene as a saturable absorber for ultrafast pulsed lasers. *Adv Funct Mater*, 19(19):3077-3083. https://doi.org/10.1002/adfm.200901007

Bonaccorso F, Sun Z, Hasan T, et al., 2010. Graphene photonics and optoelectronics. *Nat Photon*, 4(9):611-622. https://doi.org/10.1038/nphoton.2010.186

Cao WJ, Wang HY, Luo AP, et al., 2012. Graphene-based, 50 nm wide-band tunable passively Q-switched fiber laser. *Laser Phys Lett*, 9(1):54-58. https://doi.org/10.1002/lapl.201110085

Chen SQ, Zhao CJ, Li Y, et al., 2014. Broadband optical and microwave nonlinear response in topological insulator. *Opt Mater Expr*, 4(4):587-596. https://doi.org/10.1364/OME.4.000587

Chen Y, Zhao CJ, Chen SQ, et al., 2014. Large energy, wavelength widely tunable, topological insulator Q-switched erbium-doped fiber laser. *IEEE J Sel Top Quant Electron*, 20(5):315-322. https://doi.org/10.1109/jstqe.2013.2295196

Garmire E, 2000. Resonant optical nonlinearities in semiconductors. *IEEE J Sel Top Quant Electron*, 6(6):1094- 1110. https://doi.org/10.1109/2944.902158

Guo J, Zhang Y, Wang ZH, et al., 2020. Tellurium@Selenium core-shell hetero-junction: facile synthesis, nonlinear optics, and ultrafast photonics applications towards mid-infrared regime. *Appl Mater Today*, 20:100657. https://doi.org/10.1016/j.apmt.2020.100657

Guo PL, Li XH, Feng TC, et al., 2020. Few-layer bismuthene for coexistence of harmonic and dual wavelength in a mode-locked fiber laser. *ACS Appl Mater Interf*, 12(28): 31757-31763. https://doi.org/10.1021/acsami.0c05325

Hisyam MB, Rusdi MFM, Latiff AA, et al., 2017. Generation of mode-locked Ytterbium doped fiber ring laser using few-layer black phosphorus as a saturable absorber. *IEEE J Sel Top Quant Electron*, 23(1):39-43. https://doi.org/10.1109/JSTQE.2016.2532270

Hsieh D, Qian D, Wray L, et al., 2008. A topological Dirac insulator in a quantum spin Hall phase. *Nature*, 452(7190): 970-974. https://doi.org/10.1038/nature06843

Huang HY, Qiu M, Li Q, et al., 2016. Donor–acceptor conjugated polymers based on thieno[3,2-b]indole (TI) and 2,1,3-benzothiadiazole (BT) for high efficiency polymer solar cells. *J Mater Chem C*, 4(23):5448-5460. https://doi.org/10.1039/C6TC00929H

Huang WC, Xie ZJ, Fan TJ, et al., 2018a. Black-phosphorus-analogue tin monosulfide: an emerging optoelectronic two-dimensional material for high-performance photodetection with improved stability under ambient/harsh conditions. *J Mater Chem C*, 6(36): 9582-9593. https://doi.org/10.1039/C8TC03284J

Huang WC, Xing CY, Wang YZ, et al., 2018b. Facile fabrication and characterization of two-dimensional bismuth(III) sulfide nanosheets for high-performance photodetector applications under ambient conditions. *Nanoscale*, 10(5):2404-2412. https://doi.org/10.1039/C7NR09046C

Huang WC, Zhang Y, You Q, et al., 2019. Enhanced photodetection properties of Tellurium@Selenium roll-to-roll nanotube heterojunctions. *Small*, 15(23):e1900902. https://doi.org/10.1002/smll.201900902

Huang WC, Ma CY, Li C, et al., 2020. Highly stable MXene (V_2CT_x)-based harmonic pulse generation. *Nanophotonics*, 9(8):2577-2585. https://doi.org/10.1515/nanoph-2020-0134

Huang YZ, Luo ZQ, Li YY, et al., 2014. Widely-tunable, passively Q-switched erbium-doped fiber laser with few-layer MoS_2 saturable absorber. *Opt Expr*, 22(21):25258-25266. https://doi.org/10.1364/OE.22.025258

Jhon YI, Lee J, Jhon YM, et al., 2018. Topological insulators for mode-locking of 2-μm fiber lasers. *IEEE J Sel Top Quant Electron*, 24(5):1102208. https://doi.org/10.1109/JSTQE.2018.2811903

Kowalczyk M, Bogusławski J, Zybała R, et al., 2016. Sb_2Te_3-deposited D-shaped fiber as a saturable absorber for mode-locked Yb-doped fiber lasers. *Opt Mater Expr*, 6(7): 2273-2282. https://doi.org/10.1364/ome.6.002273

Li XH, Peng JJ, Liu RS, et al., 2020. Fe_3O_4 nanoparticle-enabled mode-locking in an erbium-doped fiber laser. *Front Optoelectron*, 13(2):149-155. https://doi.org/10.1007/s12200-020-1057-4

Liang D, Huang X, Kurczveil G, et al., 2016. Integrated finely tunable microring laser on silicon. *Nat Photon*, 10(11): 719-722. https://doi.org/10.1038/nphoton.2016.163

Lin YH, Lin SF, Chi YC, et al., 2015. Using n- and p-type Bi_2Te_3 topological insulator nanoparticles to enable controlled femtosecond mode-locking of fiber lasers. *ACS Photon*, 2(4):481-490.

https://doi.org/10.1021/acsphotonics.5b00031

Liu J, Liu S, Wei JS, 2010. Origin of the giant optical nonlinearity of Sb_2Te_3 phase change materials. *Appl Phys Lett*, 97(26):261903. https://doi.org/10.1063/1.3530428

Liu WJ, Pang LH, Han HN, et al., 2015. Generation of dark solitons in erbium-doped fiber lasers based Sb_2Te_3 saturable absorbers. *Opt Expr*, 23(20):26023-26031. https://doi.org/10.1364/OE.23.026023

Liu WJ, Pang LH, Han HN, et al., 2016. 70-fs mode-locked erbium-doped fiber laser with topological insulator. *Sci Rep*, 6:19997. https://doi.org/10.1038/srep19997

Liu WJ, Liu ML, Han HN, et al., 2018. Nonlinear optical properties of WSe_2 and $MoSe_2$ films and their applications in passively Q-switched erbium doped fiber lasers. *Photon Res*, 6(10):C15-C21. https://doi.org/10.1364/PRJ.6.000C15

Lü YJ, Wei C, Zhang H, et al., 2019. Wideband tunable passively Q-switched fiber laser at 2.8 μm using a broadband carbon nanotube saturable absorber. *Photon Res*, 7(1): 14-18. https://doi.org/10.1364/PRJ.7.000014

Luo ZC, Liu M, Liu H, et al., 2013. 2 GHz passively harmonic mode-locked fiber laser by a microfiber-based topological insulator saturable absorber. *Opt Lett*, 38(24):5212-5215. https://doi.org/10.1364/OL.38.005212

Meng YC, Salhi M, Niang A, et al., 2015. Mode-locked Er:Yb-doped double-clad fiber laser with 75-nm tuning range. *Opt Lett*, 40(7):1153-1156. https://doi.org/10.1364/OL.40.001153

Popa D, Sun Z, Hasan T, et al., 2011. Graphene Q-switched, tunable fiber laser. *Appl Phys Lett*, 98(7):073106. https://doi.org/10.1063/1.3552684

Qiu M, Long SR, Li BX, et al., 2013. Toward an understanding of how the optical property of water-soluble cationic polythiophene derivative is altered by the addition of salts: the hofmeister effect. *J Phys Chem C*, 117(42):21870-21878. https://doi.org/10.1021/jp407430y

Qiu M, Brandt RG, Niu YL, et al., 2015. Theoretical study on the rational design of cyano-substituted P3HT materials for OSCs: substitution effect on the improvement of photovoltaic performance. *J Phys Chem C*, 119(16):8501-8511. https://doi.org/10.1021/acs.jpcc.5b01071

Qiu M, Zhu DQ, Yan LY, et al., 2016. Strategy to manipulate molecular orientation and charge mobility in D–A type conjugated polymer through rational fluorination for improvements of photovoltaic performances. *J Phys Chem C*, 120(40):22757-22765. https://doi.org/10.1021/acs.jpcc.6b03756

Rong XF, Luo SY, Li WS, et al., 2018. Dual-wavelength Bi_2Se_3-based passively Q-switching Nd^{3+}-doped glass all-fiber laser. *Chin Opt Let*, 16(2):020016. https://doi.org/10.3788/col201816.020016

Sotor J, Sobon G, Grodecki K, et al., 2014a. Mode-locked erbium-doped fiber laser based on evanescent field interaction with Sb_2Te_3 topological insulator. *Appl Phys Lett*, 104(25):251112. https://doi.org/10.1063/1.4885371

Sotor J, Sobon G, Macherzynski W, et al., 2014b. Mode-locking in Er-doped fiber laser based on mechanically exfoliated Sb_2Te_3 saturable absorber. *Opt Mater Expr*, 4(1):1-6. https://doi.org/10.1364/OME.4.000001

Wang JT, Yin JD, He TC, et al., 2018. Sb_2Te_3 mode-locked ultrafast fiber laser at 1.93 μm. *Chin Phys B*, 27(8): 084214. https://doi.org/10.1088/1674-1056/27/8/084214

Wang T, Jin XX, Yang J, et al., 2019a. Ultra-stable pulse generation in ytterbium-doped fiber laser based on black phosphorus. *Nanoscale Adv*, 1(1):195-202. https://doi.org/10.1039/c8na00221e

Wang T, Shi XY, Wang J, et al., 2019b. Nonlinear photoresponse of metallic graphene-like VSe_2 ultrathin nanosheets for pulse laser generation. *Sci China Inform Sci*, 62(12):220406. https://doi.org/10.1007/s11432-019-2677-9

Wang T, Jin XX, Yang J, et al., 2019c. Oxidation-resistant black phosphorus enable highly ambient-stable ultrafast pulse generation at a 2 μm Tm/Ho-doped fiber laser. *ACS Appl Mater Interf*, 11(40):36854-36862. https://doi.org/10.1021/acsami.9b12415

Wang T, Wu J, Wu HS, et al., 2019d. Wavelength-tunable LP_{11} mode pulse fiber laser based on black phosphorus. *Opt Laser Technol*, 119:105618. https://doi.org/10.1016/j.optlastec.2019.105618

Wang YZ, Huang WC, Wang C, et al., 2019. An all-optical, actively Q-switched fiber laser by an antimonene-based optical modulator. *Laser Photon Rev*, 13(4):1800313. https://doi.org/10.1002/lpor.201800313

Wang ZH, Li CY, Ye JW, et al., 2019. Generation of harmonic mode-locking of bound solitons in the ultrafast fiber laser with Sb_2Te_3 saturable absorber on microfiber. *Laser Phys Lett*, 16(2):025103. https://doi.org/10.1088/1612-202x/aaf790

Woodward RI, Kelleher EJR, Howe RCT, et al., 2014. Tunable Q-switched fiber laser based on saturable edge-state absorption in few-layer molybdenum disulfide (MoS_2). *Opt Expr*, 22(25):31113-31122. https://doi.org/10.1364/OE.22.031113

Wu HS, Wu J, Yu Q, et al., 2017. Over 70 nm broadband-tunable Yb-doped fiber pulse laser based on trilaminar graphene. *Laser Phys Lett*, 14(6):065105. https://doi.org/10.1088/1612-202X/aa6f86

Wu LM, Xie ZJ, Lu L, et al., 2018. Few-layer tin sulfide: a promising black-phosphorus-analogue 2D material with exceptionally large nonlinear optical response, high stability, and applications in all-optical switching and wavelength conversion. *Adv Opt Mater*, 6(2):1700985. https://doi.org/10.1002/adom.201700985

Wu Q, Huang WC, Wang YZ, et al., 2020. All-optical control of microfiber knot resonator based on 2D Ti_2CT_x MXene. *Adv Opt Mater*, 8(7):1900977. https://doi.org/10.1002/adom.201900977

Xia HD, Li HP, Lan CY, et al., 2015. Few-layer MoS_2 grown by chemical vapor deposition as a passive Q-switcher for tunable erbium-doped fiber lasers. *Photon Res*, 3(3):A92-A96. https://doi.org/10.1364/PRJ.3.000A92

Xie ZJ, Zhang F, Liang ZM, et al., 2019. Revealing of the ultrafast third-order nonlinear optical response and enabled photonic application in two-dimensional tin sulfide. *Photon Res*, 7(5):494-502. https://doi.org/10.1364/PRJ.7.000494

Xing CY, Xie ZJ, Liang ZM, et al., 2017. 2D nonlayered selenium nanosheets: facile synthesis, photoluminescence, and ultrafast photonics. *Adv Opt Mater*, 5(24):1700884. https://doi.org/10.1002/adom.201700884

Xiong Q, 2019. Two-dimensional materials: new opportunities for electronics, photonics and optoelectronics. *Sci Bull*, 64(15):1031-1032. https://doi.org/10.1016/j.scib.2019.07.010

Yan PG, Chen H, Li KY, et al., 2016. Q-switched fiber laser using a fiber-tip-integrated TI saturable absorption mirror. *IEEE Photon J*, 8(1):1500506. https://doi.org/10.1109/JPHOT.2015.2509864

Yang YY, Yang S, Li C, et al., 2019. Passively Q-switched and mode-locked Tm-Ho co-doped fiber laser using a WS_2 saturable absorber fabricated by chemical vapor deposition. *Opt Laser Technol*, 111:571-574. https://doi.org/10.1016/j.optlastec.2018.10.023

Zhang H, Tang DY, Knize RJ, et al., 2010. Graphene mode locked, wavelength-tunable, dissipative soliton fiber laser. *Appl Phys Lett*, 96(11):111112. https://doi.org/10.1063/1.3367743

Zhang H, Virally S, Bao QL, et al., 2012. Z-scan measurement of the nonlinear refractive index of graphene. *Opt Lett*, 37(11):1856-1858. https://doi.org/10.1364/OL.37.001856

Zhang HJ, Liu CX, Qi XL, et al., 2009. Topological insulators in Bi_2Se_3, Bi_2Te_3 and Sb_2Te_3 with a single Dirac cone on the surface. *Nat Phys*, 5(6):438-442. https://doi.org/10.1038/nphys1270

Zhang Q, Jiang XT, Zhang M, et al., 2020. Wideband saturable absorption in metal–organic frameworks (MOFs) for mode-locking Er- and Tm-doped fiber lasers. *Nanoscale*, 12(7):4586-4590. https://doi.org/10.1039/C9NR09330C

Zhang Y, Zhang F, Xu YG, et al., 2019. Epitaxial growth of topological insulators on semiconductors (Bi_2Se_3/Te@Se) toward high-performance photodetectors. *Small Methods*, 3(12):1900349. https://doi.org/10.1002/smtd.201900349

Zhang Y, You Q, Huang WC, et al., 2020a. Few-layer hexagonal bismuth telluride (Bi_2Te_3) nanoplates with high-performance UV-Vis photodetection. *Nanoscale Adv*, 2(3):1333-1339. https://doi.org/10.1039/D0NA00006J

Zhang Y, Huang P, Guo J, et al., 2020b. Graphdiyne-based flexible photodetectors with high responsivity and detectivity. *Adv Mater*, 32(23):2001082. https://doi.org/10.1002/adma.202001082

Zhang Y, Guo J, Xu YG, et al., 2020c. Synthesis and optoelectronics of mixed-dimensional Bi/Te binary heterostructures. *Nanoscale Horiz*, 5(5):847-856. https://doi.org/10.1039/C9NH00805E